Effect of Low-Dose 18F-FDG on Image Quality in Digital PET/CT

Yuya Shirakawa (have_a_nice_day544@yahoo.co.jp)
Kyorin University Hospital

Original research

Keywords: digital PET/CT, dose, phantom, semiconductor, 18F-FDG

Posted Date: January 18th, 2022

DOI: https://doi.org/10.21203/rs.3.rs-1204228/v1

Effect of Low-Dose ^{18}F-FDG on Image Quality in Digital PET/CT

Yuya Shirakawa[1]

[1]**Department of Radiology, Kyorin University Hospital, Tokyo, Japan**

Correspondence

Yuya Shirakawa
Radiological Technologist

Department of Radiology, Kyorin University Hospital,
6-20-2 Shinkawa, Mitaka, Tokyo, Japan 181-8611

E-mail: have_a_nice_day544@yahoo.co.jp
Tel: +81-422-47-5511
Fax: +81-422-76-0361

Abstract

Patients in Japan undergoing PET/CT are injected with 3.7 MBq of ^{18}F-FDG which is a standard based on outdated instrumentation. We investigated whether informative ^{18}F-FDG-PET/CT images of tumor glucose metabolism could be acquired with lower ^{18}F doses.

Methods

The background activity of a NEMA body phantom with 10–37-mm hot spheres containing ^{18}F-FDG was set at 2.53 kBq/mL (= 3.7 MBq/kg dose; Hot/BG = 4; standard), and 1.73 and 1.34 kBq/mL (= 2.5 and 2.0 MBq/kg doses, respectively). Images were reconstructed using TOF-3D-OSEM and a Gaussian filter (GF) (FWHM 4 mm) and Clear adaptive Low-noise Method (CaLM Mild). Image quality was evaluated as % background variability ($N_{B,10mm}$), % contrast of 10-mm hot sphere ($Q_{H,10\ mm}$), background coefficients of variation ($CV_{background}$), ratios of $Q_{H,10mm}$ to $N_{B,10\ mm}$ ($Q_{H,10\ mm}/N_{B,10\ mm}$), and recovery coefficients (RC). The detectability of 10 mm hot spheres was evaluated at each dose.

Results

The $N_{B,10\ mm}$ on images of 3.7 MBq/kg doses acquired for 270 sec was 5.5% (GF and CaLM Mild), which met the guideline standard (< 5.6%), and 6.9% and 7.6% (GF) at 2.5 and 2.0 MBq/kg respectively, on images acquired for 300 sec, and 7.1% and 7.4% (CaLM Mild), which exceeded the standard.

The $Q_{H,10\ mm}$ indicated better contrast on images acquired for 120 sec (clinical standard), with CaLM Mild, than the GF. The $CV_{background}$ values for 3.7 MBq/kg dose equivalents were 9.9% (GF) and 10% (CaLM Mild) respectively, for images acquired for 270 and 300 sec, which met the guideline criterion (≤ 10%), and 11% and 12% (GF), and

13% (CaLM Mild) for 2.5 and 2.0 MBq/kg doses for images acquired for 300 sec. The $Q_{H,10\ mm}/N_{B,10\ mm}$ values at 2.0 MBq/kg for images acquired for 120 sec were 3.8 (GF) and 3.5 (CaLM Mild), which met the criterion (> 2.8), and the RCs of 0.73 (GF) and 0.98 (CaLM Mild) for the 10-mm hot sphere, also satisfied the criterion (> 0.38). Visual detectability at all doses met the criterion at 120 sec.

Conclusions

The quality of semiconductor digital PET/CT images was good at doses below the current standard.

Key words: digital PET/CT, dose, phantom, semiconductor, ^{18}F-FDG

Background

Positron emission tomography (PET) using 2-deoxy-2[^{18}F]fluoro-D-glucose (^{18}F-FDG) is widely applied to diagnose cancer and evaluate therapeutic effects (*1,2*) .

Newer digital PET/computed tomography (PET/CT) systems include semiconductor devices for detectors. The digital semiconductor. “Cartesion Prime” PET system (Canon Medical Systems Corp., Otawara, Japan) was installed in our hospital during November 2020, and it has since been applied to stage and diagnose tumor recurrence and metastasis (*3*). This system uses cerium-doped lutetium yttrium orthosilicate (LYSO) scintillators, silicon photomultipliers (SiPM) semiconductor photosensors as detectors, and photomultiplier tubes. The system delivers better image quality over shorter acquisition periods than conventional analog PET systems that have photomultiplier tubes. One feature of the new system is that the scintillator and semiconductor device are coupled in a one-to-one structure, which eliminates the need for positional (Anger) calculation, and the time of flight (TOF) time resolution

is far better than that of analog PET systems, resulting in improved sensitivity.

A diagnostic reference level (DRL) has been proposed to internationally optimize radiation protection (*4*). Patients would benefit from lower doses of radiation, whereas high doses that are unnecessary for diagnosis are harmful to patients. However, a minimum dose for image acquisition has not been established. The standard dose of ^{18}F-FDG required to assess tumor glucose metabolism on ^{18}F PET/CT images is 3.7 MBq/kg according to the current Japanese guidelines (*5*). However, this standard has not significantly changed since the early 2000s, when analog PET/CT was the mainstream, whereas digital PET/CT is becoming more prevalent (*6*). Digital PET/CT is likely to provide better image quality at lower doses than conventional PET/CT because of the features described above. Therefore, the present study aimed to determine whether the quality of digital ^{18}F-FDG PET/CT images of tumor glycolytic metabolism could be maintained at doses below the current guidelines using phantoms (*7,8*).

1. Methods

1.1 Equipment used and phantom preparation

The PET/CT system was a Cartesion Prime (Canon Medical Systems Corp., Otawara, Japan) equipped with an 80-row multidetector CT system. Table 1 shows the feature of this system. The analysis software used was PET quactIE (Nihon Medi-Physics Co., Tokyo, Japan). The phantom was a NEMA IEC body phantom with 10–37-mm spheres.

Table 1. Characteristics of semiconductor digital PET/CT systems.

PET characteristics	Cartesion Prime
Detector material	LYSO(Lu-based)
Crystal size	4.1×4.1×20 mm
Detector diameter	780 mm
Axial field of view	270 mm
Number of image planes	128
Sensitivity	13.0 cps/kBq
TOF resolution	< 280 ps

1.2 PET /CT imaging and image reconstruction

According to the Japanese guidelines, the background radioactivity concentration in the region is 2.53 kBq/mL when 3.7 MBq/kg of ^{18}F-FDG is administered to a person weighing 60 kg (standard body weight in Japan), and images are acquired from 1 hour thereafter (*8*). We designed a phantom with background levels of 2.53, 1.73, and 1.34 kBq/mL (equivalent to 3.7 [standard], 2.5, and 2.0 MBq/kg doses, respectively) with spheres containing 4-fold more ^{18}F radioactivity than each background.

Images were acquired from the phantom in list-mode for 30 minutes and cut out at intervals of 30 sec/bed in the range of 30–300 sec/bed to evaluate image quality. The data were reconstructed at 30 min/bed for quantitative evaluation. Images were reconstructed using three-dimensional Ordered Subset Expectation Maximization (3D-OSEM) with 12 subsets, 3 iterations, a 336 × 336 matrix and 2.11-mm pixels. Computed tomography attenuation was corrected using TOF, and noise was processed using a Gaussian filter at FWHM 4 mm and the Clear adaptive Low-noise Method (CaLM) , which is based on the non-local-mean (NLM) method (*9*). The CT imaging conditions were as follows: tube voltage 120 kV, tube current volume exposure control, collimation 0.5 mm × 80, scan speed

0.5 s, and slice thickness 2.0 mm.

1.3 Evaluation indices

The ability to draw a 10-mm hot sphere and image noise characteristics in the background was evaluated. The following physical indices were calculated: % background variability ($N_{B,10\ mm}$), %contrast of a 10-mm hot sphere ($Q_{H,10\ mm}$), coefficient of variation of the background ($CV_{background}$), and the ratio of $Q_{H,10\ mm}$ to $N_{B,10\ mm}$ ($Q_{H,10\ mm}/N_{B,10\ mm}$). The recovery coefficient (RC) of each sphere was calculated using the data derived from 30 min/bed.

The RC was calculated by placing a region of interest (ROI) in the slice with the most hot spheres (Figure 1) as follows.

$$RC = \frac{C_j}{C_{37\ mm}} \qquad \text{Eq. 1.}$$

where Cj is the maximum total value for each hot sphere and $C_{37\ mm}$ is the maximum total for the 37-mm sphere. Twelve circular ROIs of 10 mm spheres were placed on five slices (± 1 and ± 2 cm) where each hot sphere was most clearly evident (Figure 1), then $N_{B,10\ mm}$ was calculated using the average of the coefficient of variation for each slice as:

$$N_{B,10\ mm} = \frac{SD_{10\ mm}}{C_{B,10\ mm}} \times 100\% \qquad \text{Eq. 2.}$$

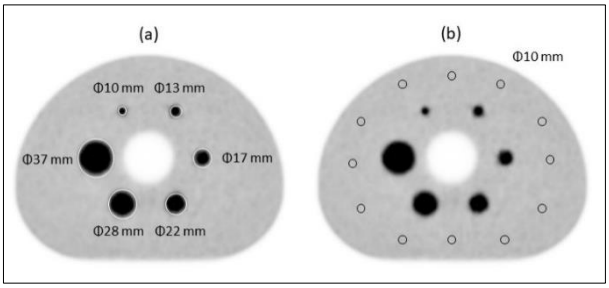

Figure 1. ROI placement.

Layouts for (a) SUV and RC, and (b) $N_{B,10\ mm}$ measurements.

Here, $SD_{B,10\ mm}$ is the standard deviation in each ROI set in the background (BG), and $C_{B,10\ mm}$ and $SD_{10\ mm}$ represent the average count and the standard deviation in the ROI with a diameter of 10 mm in the BG. The $SD_{10\ mm}$ is calculated as:

$$SD_{\ j} = \sqrt{\frac{\sum_{K=1}^{K}(C_{B,j,k}-C_{B,j})^2}{(K-1)}} \qquad \text{Eq. 3.}$$

where j is 10 mm and K is 60 (12 ROIs on five slices, 60 in total). The $Q_{H,10\ mm}$ was calculated by measuring the 10-mm hot sphere and the BG using a circular ROI with a diameter of 10 mm in a slice where the hot sphere was the most clearly evident as:

$$Q_{H,10\ mm} = \frac{C_{H,10\ mm}/C_{H,10\ mm}-1}{\alpha_H/\alpha_B-1} \times 100\% \qquad \text{Eq. 4.}$$

where $Q_{H,10\ mm}$ is the average pixel value in the ROI for the 10 mm hot sphere, $C_{B,10\ mm}$ is the average pixel value in the BG calculated from the circular ROI of the 12 spheres with a diameter of 10 mm, and α_H and α_B are the radioactivity concentrations (Bq/mL), in the hot sphere and BG, respectively. Twelve circular ROIs of 37-mm spheres were set in the BG where a slice contained clear representations of all sizes of spheres to determine $CV_{background}$. Similar circular ROIs were also set in slices ± 1 and ± 2 cm away from that slice (total slices, n = 5). Counts in each ROI were calculated as:

$$CV_{background} = mean\ of \left[\frac{SD_{37\ mm}}{C_{B,37\ mm}} \times 100 \right] \% \quad \text{Eq. 5.}$$

Here, $C_{B,37\ mm}$ and $SD_{37\ mm}$ are the mean counts and standard deviation, respectively, in each ROI of 37-mm spheres in the BG. The SD_{37mm} in each ROI was calculated using Eq. 3, where j is 37 mm and k is the number of pixels in each ROI. Five radiologists and a nuclear medicine specialist visually evaluated the ability to define the 10-mm hot sphere on reconstructed images from 30–300 at 30-sec intervals using a workstation terminal for reading clinical PET images. Images were displayed using an invert grayscale as the color look-up table. The lower and upper limits of the display window level were fixed at SUV = 0 and 4, respectively. All image slices were visually evaluated by sequentially displaying the images acquired over the shortest period. Visibility of the 10-mm hot sphere was scored from 0 to 2 as not identifiable, identifiable with noise and identifiable, respectively. When > 50% of the evaluators judged the 10-mm hot sphere as identifiable, an average score of ≥ 1.5 was taken as the criterion for satisfying the evaluation (*7*).

2. Results

2.1 $N_{B,10\ mm}$

Figures 2 and 3 show the relationship between $N_{B,10\ mm}$ and dose. The noise trends were similar between the Gaussian filter and CaLM Mild from 30 to 300 sec, and the noise increased with decreasing dose. The 3.7 MBq/kg dose was 5.5% for the Gaussian filter and 5.5% for CaLM Mild on images acquired for 270 s, which satisfied the guideline value of < 5.6% (*7,8*). At doses of 2.5 and 2.0 MBq/kg, the respective $N_{B,10\ mm}$ values determined from images acquired over 300 sec were 6.9% and 7.6%, for the Gaussian filter, and 7.1% and 7.4% for CaLM Mild. These results did not meet the guideline values.

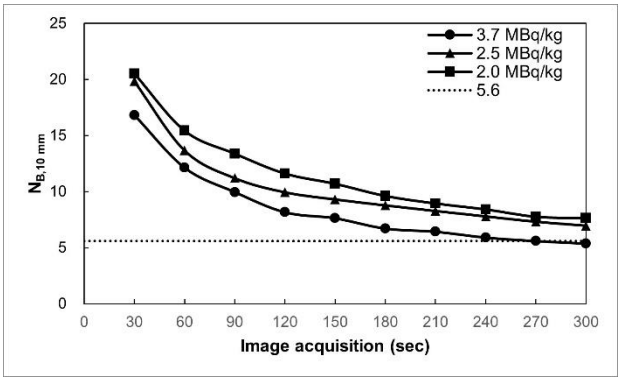

Figure 2. $N_{B,10\ mm}$ Gaussian filter FWHM = 4.

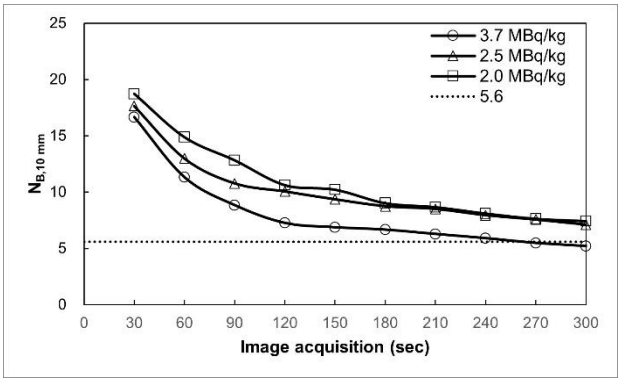

Figure 3. $N_{B,10\ mm}$ CaLM Mild.

2.2 $Q_{H,10\ mm}$

Figures 4 and 5 show the relationship between $Q_{H,10\ mm}$ and doses of 2.0, 2.5, and 3.7 MBq/kg. Values for $Q_{H,10\ mm}$ were higher in the Gaussian filter after acquisition for 120 s. Values were higher for CaLM Mild in the order of 2.0, 3.7, and 2.5 MBq/kg doses in images acquired for 120–240 sec, and the order of 2.5, 2.0, and 3.7 MBq/kg between 240 and 300 sec thereafter. Values determined using CaLM Mild surpassed those in the Gaussian filter at 120 sec, and $Q_{H,10\ mm}$ continued to increase until 300 sec.

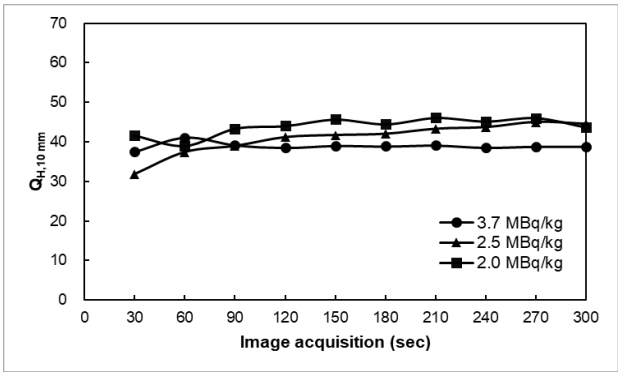

Figure 4. $Q_{H,10\ mm}$ Gaussian filter FWHM = 4.

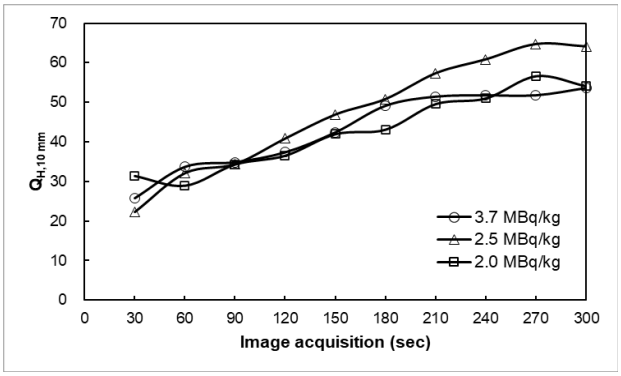

Figure 5. $Q_{H,10\ mm}$ CaLM Mild.

2.3 $CV_{background}$

Figures 6 and 7 show the relationship between $CV_{background}$ and dose. The trends for the Gaussian filter and CaLM Mild were similar between 30 and 300 sec. At a dose of 3.7 MBq/kg, The CV background was 9.9% and 10% for the Gaussian filter in images collected for 270 s, and ≤ 10% for CaLM Mild when images were acquired for 300 sec (8). However, at doses of 2.5 and 2.0 MBq/kg, $CV_{background}$ values were 11% and 12% for the Gaussian filter, and 13% for CaLM Mild, respectively, when images were acquired for 300 sec. These results did not meet the guideline values.

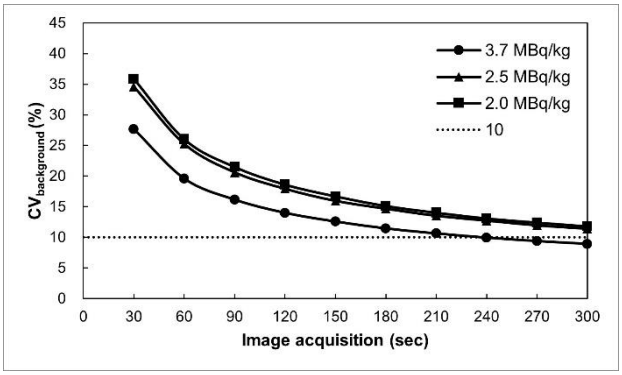

Figure 6. $CV_{background}$ Gaussian filter FWHM = 4.

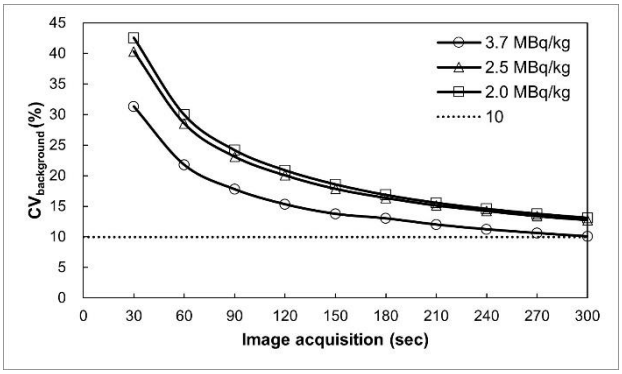

Figure 7. $CV_{background}$ CaLM Mild.

2.4 $Q_{H,10\ mm}/N_{B,10\ mm}$

Figures 8 and 9 show the relationship between $Q_{H,10\ mm}/N_{B,10\ mm}$ and dose. The trends in these values were similar between the Gaussian filter and CaLM Mild between images acquired for 30 to 300 sec and increased along with the dose. When the dose was 3.7 MBq/kg and images were acquired for 60 s, the $Q_{H,10\ mm}/N_{B,10\ mm}$ determined using the Gaussian filter and CaLM Mild were 3.4 and 3.0, respectively, which satisfied the guideline standard of > 2.8. When the dose was 2.0 MBq/kg and the acquisition duration was 120 sec, the values obtained using the Gaussian filter and CaLM Mild were 3.8 and 3.5, respectively, which exceeded the reference values (*7, 8*).

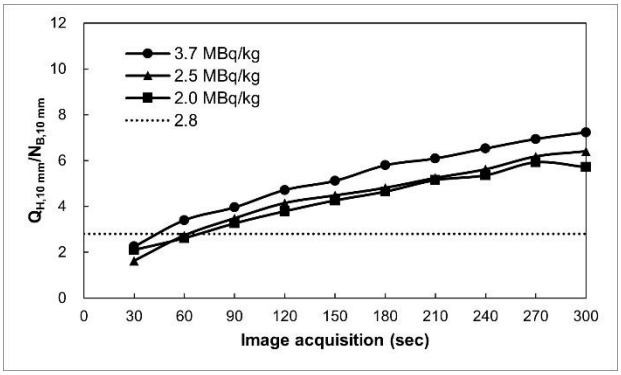

Figure 8. $Q_{H,10\ mm}/N_{B,10\ mm}$ Gaussian filter FWHM = 4.

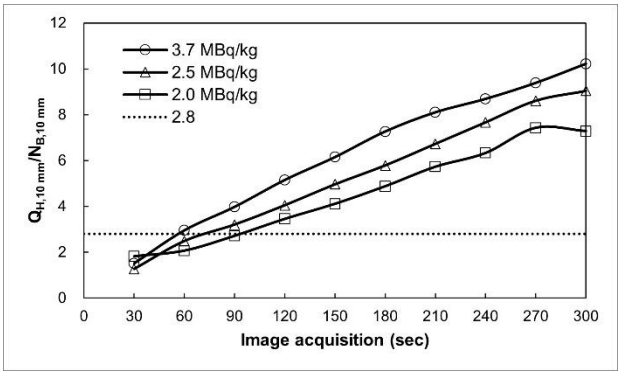

Figure 9. $Q_{H,10\ mm}/N_{B,10\ mm}$ CaLM Mild.

2.5 Recovery coefficients

Figures 10 and 11 show the relationship between RC and dose.

Recovery coefficients determined for 10-mm hot spheres equivalent to a dose of 2.0 MBq/kg using the Gaussian filter and CaLM Mild were high at 0.73 and 0.98, respectively. All other concentrations of the hot spheres exceeded the guideline standard of > 0.38 (*7*,*8*).

In addition, the partial volume effect (PVE) determined using the Gaussian filter was improved by 34% from 0.73 to 0.98 at 2.0 MBq/kg in CaLM Mild.

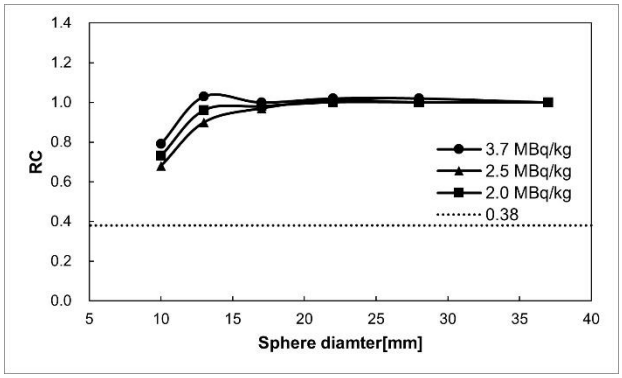

Figure 10. Recovery coefficients: Gaussian filter FWHM = 4.

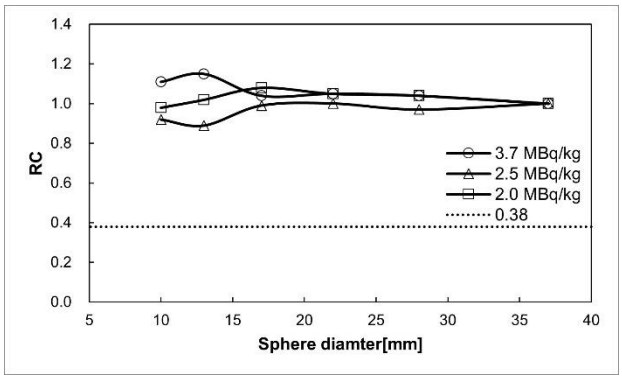

Figure 11. Recovery coefficients CaLM Mild

2-6 Visual evaluation of detectability

The ability of the Gaussian filter (FWHM 4 mm) and CaLM Mild to visualize the 10-mm hot sphere at 3.7, 2.5 and 2.0 MBq/kg doses met the standard at 60, 90, and 120 seconds, respectively (Table 2, Fig. 12).

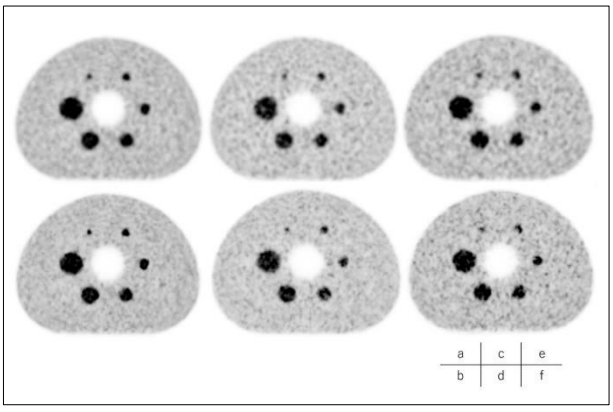

Figure 12. PET images acquired from body phantom for 120 sec. Upper and lower rows, Gaussian filter at FWHM 4 mm and CaLM Mild, respectively. Equivalent to doses of (a, b) 3.7, (c, d) 2.5, (e, f), 2.0 MBq/kg.

253 **Table 2.** Visual evaluation of detectability.

254

Dose (MBq/kg)	Reconstruction mode	Acquisition period (sec)									
		30	60	90	120	150	180	210	240	270	300
3.7	GF	1.4	2	2	2	2	2	2	2	2	2
	CaLM Mild	0.8	2	2	2	2	2	2	2	2	2
2.5	GF	0	0.8	1.6	2	2	2	2	2	2	2
	CaLM Mild	0	1	1.8	1.8	2	2	2	2	2	2
2.0	GF	0	0.8	1	2	2	2	2	2	2	2
	CaLM Mild	0.2	0.4	1.2	1.8	2	2	2	2	2	2

255 GF, Gaussian filter (FWHM 4 mm)

256

257 ## Discussion

258 The present study investigated the ability of a semiconductor digital PET/CT system to generate quality images

259 from a phantom with simulated standard and low doses (4).

260 The results for $N_{B,10mm}$ show that the noise characteristics required 270 sec to meet the guideline standard even at a

261 dose equivalent to 3.7 MBq/kg. In this system, the detector is large (270 mm in the body axis direction), and an

262 increase in random components is a problem. The probability of an accidental coincidence is proportional to the

263 width of the coincidence window.

264 The ability of the Gaussian filter and CaLM Mild to visualize the 10-mm hot sphere at doses of 3.7, 2.5, and 2.0

265 MBq/kg met the guideline standard at 60, 90, and 120 sec, respectively (Fig. 12; Table 2).

266 To cope with this problem, the coincidence coefficient window was narrowed to 3.2 nsec to eliminate more

267 coincidences. More sensitive PET detection is associated with lower contrast. If the number of contingent

268 coincidences is smaller than the true number of coincidences, the image has good contrast. Therefore, the detection

sensitivity is thought to be maximal at ~ 240 s, and a dose of 3.7 MBq/kg is required to meet the reference value of $N_{B,10\ mm}$. The $Q_{H,10\ mm}$ depended on the radioactivity concentration in the BG for the Gaussian filter. That is, the variability was large at a lower dose and acquisition periods of 30–90 sec but decreased when either the acquisition period or the dose was increased. These findings suggested that sufficient counts are necessary to obtain stable contrast. The Gaussian filter resulted in a higher $Q_{H,10\ mm}$ at lower doses, whereas $Q_{H,10\ mm}$ did not significantly differ with the dose in CaLM Mild. This might be because CaLM is based on the NLM method, and the difference between signal and noise is small at shorter acquisition periods. Therefore, a longer acquisition period and more counts improved the discrimination between signal and noise components in CaLM Mild, but the trend was steeper than that of the Gaussian filter. The reason for this is that Gaussian filter and CaLM Mild have the same amount of noise as indicated by the $N_{B,10\ mm}$, whereas the $Q_{H,10\ mm}$ in CaLM is based on the NLM method, which tends to increase the contrast as the acquisition period lengthens. The reason for this is that contrast continues to increase as the acquisition time increases. Visual descriptive scores of ≥ 1.5 (> 50% of the evaluators judged the 10-mm hot sphere as identifiable) were improved by extending the acquisition period, and scores tended to increase at higher, than at lower doses with shorter acquisition periods. This might be because a higher dose and longer acquisition period leads to more true coincidences that can be used for reconstructing images with better quality. However, 2.0 MBq/kg and image acquisition for 120 sec, which is the clinical practice, was sufficient to distinguish the 10-mm hot sphere, and the high contrast signal was not buried by background noise.

Conclusions

We evaluated the image quality of ^{18}F-FDG tumor glycolysis using a semiconductor digital PET/CT system at lower doses than the current standard. The evaluation of physical parameters and visual assessment of the acquired images were good even at low doses. Therefore, small (~ 10 mm) lesions should be detectable within clinical acquisition periods at doses below the current standard (4).

Abbreviations

FDG: Fluorodeoxyglucose; CT: Computed tomography; PET: Positron emission tomography; DRL: Diagnostic reference level; 3D-OSEM: three-dimensional Ordered Subset Expectation Maximization; CaLM: Clear adaptive Low-noise Method; NLM: Non-local-mean method; RC: Recovery coefficient; ROI: Region of interest; SUV: Standardized uptake value; BG: Background; SD: Standard deviation

Acknowledgements

Not applicable.

Author's contributions

Not applicable.

Author's information

Not applicable.

Funding

Not applicable.

Availability of data and materials

Not applicable.

Declarations

Ethics approval and consent to participate

This study was based on a phantom. Thus, approval by our institutional Ethics Committee was not required.

Consent for publication

Not applicable.

Competing interests

The datasets generated and analysed during the current study are not publicly available due to the large volume of DICOM data , but are available from the corresponding author on reasonable request.

Author details

Yuya Shirakawa
Radiological Technologist

Department of Radiology, Kyorin University Hospital,
6-20-2 Shinkawa, Mitaka, Tokyo, Japan 181-8611

E-mail: yuya_shirakawa@ks.kyorin-u.ac.jp
Tel: +81-422-47-5511
Fax: +81-422-76-0361

REFERENCES

1） Lu Z, Lin M, Downe P, et al. The prognostic value of mid- and post-treatment [(18) F] fluorodeoxyglucose (FDG) positron emission tomography (PET) in indolent follicular lymphoma. Ann Nucl Med 2014; 28(8): 805-811.

2） Pauwels EK, Coumou AW, Kostkiewicz M, et al. [18F]fluoro-2-deoxy-d-glucose positron emission tomography/computed tomography imaging in oncology: initial staging and evaluation of cancer therapy. Med

Princ Pract 2013; 22(5): 427-437.

3） Daisaki H, Kojima Y, et al. New digital Cartesion Prime PET/CT scanner: Image Quality and SUV Comparison with the non-digital Celesteion PET/CT scanner. Journal of Nuclear Medicine. Vol. 61(1): 2020.

4） Japan Network for Research and Information on Medical Exposure (J-RIME), et al. National diagnostic reference levels in Japan (2020) - Japan DRLs 2020-. 2020.

5） Japanese Society of Nuclear Medicine, Japanese Society of Nuclear Medicine PET Nuclear Medicine Subcommittee. FDG-PET Cancer Screening Guidelines, 3rd Edition. 2019;10

6） FDG PET, PETCT Clinical Practice Guideline 2020 The Japanese Society of Nuclear Medicine

7） Fukukita H, et al. Japanese guideline for the oncology FDG-PET/CT date acquisition protocol : synopsis of version 2.0. Ann Nucl Med 28(7):693-705,2014

8） The Japanese Society of Nuclear Medicine, Committee on PET Nuclear Medicine: Phantom Study Procedures for Whole Body PET Imaging Using 18F-FDG, 3rd Edition, 2017

9） Qi W, Xia T, Niu X, et al. A Non-Local Means Post-Filter with Spatially Adaptive Filtering Strength for Whole-Body PET. IEEE Nuclear Science Symposium and Medical Imaging Conference (NSS/MIC) 2015

10） Matsumoto K, Dasani Y, et al. Positron Emission Tomography: Image Quality Standardization and Accuracy of Quantitative Values. Journal of Japan Society of Radiological Technology 2009; 60(5): 668-680.